

Influence of Carbon-Support on Electronic Structure and Catalytic Activity of Pt Catalysts: Binding to the CO Molecule

Mehdi Mahmoodinia,[†] Per-Olof Åstrand,^{*,†} and De Chen[‡]

[†]*Department of Chemistry, NTNU, Norwegian University of Science and Technology, Trondheim, Norway*

[‡]*Department of Chemical Engineering, NTNU, Norwegian University of Science and Technology, Trondheim, Norway*

E-mail: per-olof.aastrand@ntnu.no

Abstract

Single-atom catalysts, especially with single Pt atoms, exhibit potentially improved catalytic activity as compared to metal clusters and metal surfaces. Here, the atop and bridged bondings of the CO molecule on the Pt/C system are studied. Vibrational frequencies, Mulliken populations, charge transfer, charge density differences and density of states are examined to determine the influence of the carbon support on electronic properties and catalytic activity of the Pt adatom and dimer. Comparing orbital populations and the amount of electron transfer to/from the CO molecule show that the net amount of electron transfer to the anti-bonding $2\pi^*$ orbitals of the CO molecule is higher for the supported Pt dimer than for the substrate-free Pt dimer which leads to a lower vibrational frequency and a larger C–O bond distance. The hybridization between the π orbitals of the polycyclic aromatic hydrocarbons surface and the d orbitals of the Pt adatoms is responsible for enhancing the back donation of electrons to the $2\pi^*$ orbitals of the CO molecule which results in a larger peak below the Fermi level for the $2\pi^*$ states of the CO molecule in the corresponding density of state analysis. Therefore, it can be concluded that the carbon support significantly enhances the catalytic activity of the Pt atoms in contact with the surface for activating the CO molecule. The calculated C–O vibrational stretching frequencies provide valuable guidance for experiments considering the use of atom-type catalyst as building blocks for designing new catalysts.

Introduction

Platinum is the most efficient catalyst for oxidation and reduction reactions in direct methanol fuel cells.^{1,2} The key barriers to commercialization of Pt-based fuel cells are the high price and the poor utilization efficiency of the Pt catalyst loading per unit area. Typical loadings in platinum black catalysts are about 25 mg Pt/cm².³ A way to reduce the metal requirement is to move from platinum black to carbon-supported platinum (Pt/C) catalysts³ with loadings of about 0.4–0.8 mg Pt/cm². Hence, it is desirable to reduce the size of Pt particles even to a single atom, which usually exhibit a higher surface area. Single atom catalysts, by providing single active sites at the solid surface, exhibit many fascinating characteristics, such as high activity, selectivity, and maximum atomic utilization as compared to conventional metal catalysts.^{4–6}

In a Pt/C catalyst, the carbon support plays an important role in determining the size and degree of catalyst dispersion. Due to high surface-to-volume ratio (theoretical value of 2630 m²/g), graphene is a promising candidate as a substrate for stabilizing metal nanoparticles in heterogeneous catalysis.^{7,8} Progress in experimental techniques has made it possible to study the properties of graphene-supported metal nanoparticles such as Pt, Pd and Au,^{9–12} which may offer a new type of carbon-based metal nanocomposite for the next generation of catalysts.⁹ Besides the key electrocatalytic role of the Pt catalysts in fuel cells, they have long been used as a promoter in the Fischer-Tropsch (FT) synthesis for conversion of syngas (CO + H₂) to liquid fuels.^{13–15} The Pt promoters increase the overall FT activity by increasing the reducibility of cobalt oxides, and therefore increases the availability of active metal sites.^{13,14}

Interfaces between transition metals (TM) and graphene have been investigated extensively by several theoretical and experimental techniques.^{16–22} Müller *et al.* investigated a single Pt atom, Pt dimers and trimers on highly oriented pyrolytic graphite

using a scanning tunneling microscope (STM) in air.²¹ The Pt particles were produced by evaporation of platinum onto the surface and the position of the Pt atoms were stable, without changes for many scans. By using the atomic layer deposition technique, Sun *et al.* showed that the single Pt atoms and small clusters have significantly higher catalytic activity (up to 10 times) for methanol oxidation and superior CO tolerance compared to commercial Pt/C catalysts.⁴

Based on density functional theory (DFT), Wang *et al.* examined the interface between graphene and Pd/Pt surfaces and explained the different behavior between Pd/graphene and Pt/graphene interfaces.²² Chan *et al.* investigated the adsorption of 12 different metal adatoms on graphene surface by using DFT. The interaction between groups I–III adatoms and a graphene surface has been characterized as an ionic bonding while TM adatoms, noble metals, and group IV elements exhibited covalent bonding characteristics with strong hybridization of adatom and graphene electronic states.²³

More recently, we performed dispersion-corrected DFT calculations on Pt and Co adatoms and dimers on polycyclic aromatic hydrocarbons (PAHs).^{16–18} We found that PAH substrates not only stabilizes the metal particles but also changes their electronic structure and can tune their catalytic activity. Hence, in this work, we consider the adsorption of the CO molecule on the substrate-free and PAH-supported Pt atom and dimer to investigate the effect of the carbon support on the catalytic activity of the Pt particles. The adsorption of the CO molecule on TMs, in particular platinum, has been studied extensively^{24–30} and indeed the CO–Pt₂ system is an interesting example, as the CO binding energy of its anion has been estimated from collision-induced dissociation experiments.³¹ Hence, we study the atop and bridged bondings of the CO molecule on the Pt-surface. The results are discussed based on the effect of the carbon support on the electronic properties and catalytic activity of the Pt adatom and dimer.

Computational details

All calculations were performed based on DFT with the S12g form of the generalized gradient approximation (GGA) proposed by Swart³² and implemented in the Amsterdam Density Functional (ADF) package.^{33,34} This functional is the successor of the Swart-Solà-Bickelhaupt (SSB-D) functional,^{35,36} and it includes Grimme's D3 dispersion correction.³⁷ Its performance for spin states of transition metal complexes is well documented.^{18,32,38} The relativistic effects are taken into account at the all-electron level with the zero-order-regular approximation (ZORA) approach.³⁹⁻⁴⁴ The molecular orbitals (MOs) were expanded in an uncontracted set of Slater-type orbitals (STO), based on a basis set study. This computational approach has been successful to describe the Pt/C and Co/C interactions.¹⁶⁻¹⁸

The calculations were carried out using a polycyclic aromatic hydrocarbon (PAH) molecule as a representative example for modelling a real graphene material, since bonding to PAHs represents a model for binding to the π system relatively near defects in a real graphene material. Several PAH models were investigated in our previous work and the C₅₄H₁₈ molecule was found to be a suitable model system.¹⁸ For the geometry optimization, the BFGS (Broyden-Fletcher-Goldfarb-Shanno) algorithm⁴⁵ with a convergence criterion of 10⁻⁶ a.u. on the energy and the charge density is used. Geometry optimization has been carried out without any constraints for the CO-Pt_n (n = 1, 2) complex. For the CO-Pt_n/PAH (n = 1, 2) complex, we first optimize the Pt_n/PAH (n = 1, 2) structure without any constraints to find the most stable geometry. Moreover, a frequency analysis was carried out to ensure that the stationary points are minima (only real harmonic vibrational frequencies). Then, we fixed the position of the Pt atoms along the *x*- and *y*-axes,

i.e., in the surface plane, and relaxing the distance along the *z*-axis (perpendicular to the PAH surface), and investigated the adsorption of the CO molecule on the PAH-supported Pt atom and dimers.

The adsorption energy, E_{ads} , is calculated as a measure for the strength of binding between the CO molecule and the Pt_n/PAH (n = 1, 2) complex as

$$E_{ads} = E_{CO-Pt_n/PAH} - E_{Pt_n/PAH} - E_{CO} \quad (1)$$

where $E_{CO-Pt_n/PAH}$, $E_{Pt_n/PAH}$ and E_{CO} are electronic ground state energies for the CO-Pt_n/PAH system, the Pt_n/PAH complex and a gas phase CO molecule, respectively. A more negative value of the adsorption energy indicates a stronger binding of the CO molecule to the Pt_n/PAH complex. In addition, we examined the binding energy, E_b , of the CO molecule with the Pt atom and dimer using

$$E_b = E_{CO-Pt_n} - E_{Pt_n} - E_{CO} \quad (2)$$

where E_{CO-Pt_n} and E_{Pt_n} are electronic ground state energies for the CO-Pt_n complex and Pt_n, respectively. The basis-set superposition error (BSSE) was included using the counterpoise method.⁴⁶ A zero-point vibrational energy correction has not been considered in this work. Also no entropy effects are included in this work.

The spin state is denoted with the spin multiplicity, $2S + 1$, which for example is 1 for a singlet state and 3 for a triplet state. The degree of spin contamination for a spin-unrestricted calculation is checked by evaluation of $\langle S^2 \rangle$, which ideally should be $S(S + 1)$ and thereby 0.00 for a singlet state and 2.00 for a triplet state.

The Mulliken population analysis^{47,48} and the projected density of states analysis⁴⁹ were carried out to understand the interactions between the CO molecule and the substrate-free and supported Pt atom and dimer. The charge density difference (CDD) is calculated to illustrate how the charge density changes upon adsorption of the CO molecule and also illustrate the contribution of the PAH surface to the adsorption of the CO molecule.

The Hirshfeld charge analysis^{50,51} is used to assign partial charges. This method is evaluated by numerical integration in ADF, and appear to be reliable and not very sensitive to the basis set,³³ as compared to for example Mulliken charges.

Results and Discussions

Basis set study

To select a proper basis set to describe our system, we did a basis set study using five different basis sets (TZP, TZ2P/TZ2P.4f, TZ2P, TZ2P/QZ4P and QZ4) and the S12g functional on the Pt/ovalene ($C_{32}H_{14}$) complex. In the mixed X/Y basis set, the X basis is used for the C, O and H atoms and the Y basis is used for the Pt atoms. The ovalene molecule has been successfully used as a graphene model in previous studies⁵²⁻⁵⁴ and here it only used for the basis set study and the $C_{54}H_{18}$ molecule has been used in the rest of our calculation. As shown in Figure 1, the CO adsorption energy is converged to nearly the same value for the mixed TZ2P/QZ4P and QZ4P basis sets. The BSSE is also checked, and comparing to the adsorption energy, it is small (0.11 eV) for both the QZ4P and the mixed TZ2P/QZ4P basis sets. Therefore, to save the computational time, we selected the mixed TZ2P/QZ4P basis for our calculations, where the QZ4P basis set⁵⁵ with quadruple- ζ quality and four sets of polarization functions, is used for describing the Pt atom, and the TZ2P basis set⁵⁵ with triple- ζ quality and two sets of polarization functions, is used to describe the C, O and the H atoms. The 1s electrons are kept frozen for the C atoms to speed up the calculations without affecting the accuracy of the results.

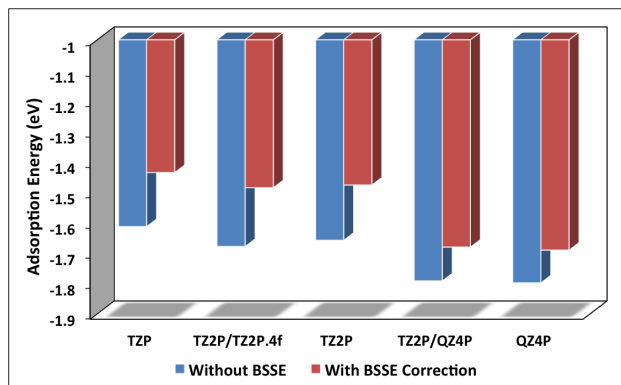


Figure 1 The CO adsorption energies with and without the BSSE correction for the Pt/ovalene complex with different basis sets. In the mixed X/Y basis set, the X basis is for the C, O and H atoms and the Y basis is for the Pt atoms. In the TZP and TZ2P basis sets, the 1s electrons are kept frozen for the C atoms.

CO interaction with Pt atom and dimer

In this section the structural, energetic and vibrational characteristics of the CO molecule interacting with the Pt atom and dimer, respectively, are investigated. The results are also compared to experimental and previous theoretical data on the CO molecule and the CO–Pt complexes to validate how well our calculations estimate the electronic and structural characteristics of these complexes, and also serves as a reference when we discuss the effect of the carbon support on the catalytic activity.

Binding of a CO molecule to a metallic surface, in particular Pt, has been studied extensively by a variety of theoretical approaches⁵⁶⁻⁶⁰ and it is usually discussed using the Dewar-Chat-Duncanson model.⁶¹⁻⁶⁴ The main characteristics of this model are a charge transfer from the lone-pair (5σ) orbital of the CO molecule to the $5d$ orbitals of the Pt atom (σ donation) and a back donation of electron density from the $5d$ orbitals of the Pt atom to the anti-bonding $2\pi^*$ orbitals of the CO molecule,⁶⁵ which is in agreement with photoelectron spectroscopy experiments.⁶⁶ The effects of the σ donation and π back donation interactions most often lead to a weakening of the C–O bond and consequently to a

lowering or red-shifting of the carbonyl stretching frequency.

However, electrostatic interactions can also provide interesting additional effects in ionized systems.^{67–71} Bauschlicher *et al.* pointed out some of the subtleties in σ donation versus electrostatic effects, and discussed how their contributions change for different systems.⁶⁹ They discuss that metal-carbonyl bonding involves a complex synergism between σ donation, electrostatic effects, and π back-bonding, but the relative importance of their contributions changes from system to system. For example, in the metal-carbonyl cations, the π back-bonding is, in general, much smaller than for the neutral species.

Molecular orbital analysis shows that both the highest occupied molecular orbitals (HOMO), 5σ , and the lowest unoccupied molecular orbitals (LUMO), $2\pi^*$, of the CO molecule are localized mainly around the C atom (Figure 2a), indicating that the CO molecule favours to bind to the metal clusters at the carbon atom. We also tried to calculate interactions at the O atom, but the CO molecule changes its direction and returns to the minimum with the C atom interacting with Pt atom. Hence, we investigate the adsorption of the CO molecule on the Pt atom and dimer at the C atom.

Furthermore, according to the CO dipole moment which point from carbon (the negative end) to oxygen (the positive end), we expect a small attraction or repulsion between the 5σ orbitals of the CO molecule and the partial charges appearing on the Pt/C system. However, the CO dipole moment is quite small and the polarity of the CO molecule may reverse when it act as a ligand, depending on the structure of the coordination complex.⁷⁰

For the CO–Pt complex, the initial structure is linear and as given in Table 1, two spin-multiplicities were examined. The singlet state is found to be the ground state with a binding energy of -3.60 eV. This value is in close agreement with the binding energy of 3.32 ± 0.52 eV determined using collision-induced dissociation experiment.³¹ The triplet state

is higher in energy by -1.51 eV, and its structure deviates from a linear structure by 12° . The bond distance of Pt–C is calculated to 1.75 Å, which is shorter than for the triplet state by 0.15 Å. For the gas phase CO molecule, the bond distance, vibrational stretching frequency (ν_{CO}) and the dipole moment are calculated to 1.135 Å, 2140.4 cm^{-1} , and 0.21 D (C^-O^+) which compare favourably with experimental values of 1.128 Å,⁷³ 2143 cm^{-1} ,⁷² and 0.12 D (C^-O^+),⁷⁷ respectively. A small elongation (0.03 Å) of the C–O bond compared to the gas phase upon adsorption on the Pt atom indicates a relocation of electrons to the anti-bonding $2\pi^*$ orbitals of the CO molecule. Reduction of ν_{CO} in the CO–Pt complex (2065.3 cm^{-1}) compared to the gas phase (2140.4 cm^{-1}) confirms the weakening of the C–O bond due to the interaction with the Pt atom.

In case of the CO–Pt₂ complex, two different structures were studied: linear (atop) and bridged structures. We find a bent structure for the atop structure in both the singlet and triplet states, which is in agreement with another theoretical study.⁵⁷ For both the atop and bridged structures, the singlet state is found to be the ground state with the triplet state higher in energy. The CO binding energy for the ground state of the bridge structure is calculated to -3.04 eV which is more stable than for the atop structure by 0.79 eV. This is in agreement with previous *ab initio* results.^{76,78–80} Multireference singles and doubles configuration interaction (MRSDCI) calculations resulted in that the bridge structure is about 0.98 eV stronger than the atop structure.⁷⁶ Collision-induced dissociation experiments also showed that the bridge structure is the most stable structure for the CO–Pt₂ anion.³¹ The dissociation energy of CO in the CO–Pt₂⁻ was reported to 3.58 ± 0.67 eV. However, a variety of experimental techniques showed that at low coverages, CO is mainly chemisorbed on the atop sites of the Pt(111) surface, and at high coverage, it is chemisorbed above both atop and bridge sites of the Pt(111) surface,^{75,81–83} although the differences between

Table 1 Results for the gas phase CO molecule and the CO interaction with Pt_n (n = 1, 2). The relative energy (E_{rel} , the energy relative to the lowest spin state), the CO binding energy, E_b , the Pt–C bond distance, d_{Pt-C} , the CO bond distance, d_{C-O} , the vibrational stretching frequency of CO, ν_{CO} , the Hirshfeld atomic charge of Pt atoms, and the calculated $\langle S^2 \rangle$ values for different spin multiplicities (2S+1) of the CO–Pt_n (n = 1, 2) complexes are given. The value in parenthesis is the atomic charge related to the Pt atom that is not connected to the CO molecule in the atop structure.

| Molecule | 2S+1 | E_{rel} (eV) | E_b (eV) | d_{Pt-C} (Å) | d_{C-O} (Å) | Pt charge (e) | ν_{CO} (cm ⁻¹) | $\langle S^2 \rangle$ |
|--------------------|------|----------------|------------------------|------------------------|--------------------|---------------------|--------------------------------|-----------------------|
| CO | 1 | 0.00 | | | 1.135 | | 2140.4 | 0.00 |
| | 3 | 5.68 | | | 1.205 | | 1779.1 | 2.01 |
| | | | | | 1.128 ^a | 2143 ^b | | |
| CO-Pt | 1 | 0.00 | -3.60 | 1.752 | 1.158 | 0.04 | 2065.3 | 0.00 |
| | 3 | 2.08 | -1.51 | 1.897 | 1.161 | 0.07 | 1948.2 | 2.00 |
| | | | | | | | | |
| CO-Pt ₂ | | | 3.32±0.52 ^c | | | | | |
| Atop | 1 | 0.00 | -2.25 | 1.804 | 1.158 | 0.057(-0.008) | 2031.5 | 0.00 |
| | 3 | 0.12 | -2.13 | 1.827 | 1.155 | 0.061(-0.017) | 2037.4 | 2.00 |
| | | | | 1.87±0.08 ^d | 1.90 ^e | 1.20 ^e | 2063 ^f | |
| | | | | 1.86 ^g | 1.14 ^g | 2029.4 ^g | | |
| Bridged | 1 | 0.00 | -3.04 | 1.90 | 1.186 | 0.090(0.090) | 1839.8 | 0.00 |
| | 3 | 0.90 | -2.14 | 1.92 | 1.180 | 0.076(0.076) | 1872.7 | 2.00 |
| | | | | | | | | |
| | | | 3.58±0.67 ^c | 1.90 ^g | 1.19 ^g | | 1840 ^f | |

^a Ref. [72] Molecular Spectra and Molecular Structure

^b Ref. [73] Physics Handbook

^c Ref. [31] Binding energies in platinum-carbonyl cluster anions using collision-induced dissociation experiment.

^d Ref. [74] Single crystal adsorption calorimetry analysis of CO on Pt(111) surface at low coverage.

^e Ref. [24] LEED intensity analysis of CO adsorbed on atop site of the Pt(111).

^f Ref. [75] Infrared reflection-absorption spectroscopy of CO adsorbed on Pt(111).

^g Ref. [76] Second-order Møller-Plesset perturbation theory.

the atop and bridged binding energies are rather small.⁷⁵ The heat of adsorption for the CO molecule on the Pt(111) surface at low coverage (atop site) is reported 1.87±0.08 eV using single crystal adsorption calorimetry.⁷⁴

The C–O bond distance and ν_{CO} are calculated to 1.158 Å (1.186 Å) and 2031.5 cm⁻¹ (1839.8 cm⁻¹) for the atop (bridge) structure, respectively. The lower ν_{CO} for the bridge structure reflects a stronger interaction between the CO molecule and the Pt dimer and consequently a stronger back donation to the anti-bonding $2\pi^*$ orbitals of the CO molecule. The Pt–C bond distance is calculated to 1.90 Å and

1.80 Å for the bridge and atop structures, respectively. Our results are in good agreement with previous studies and are compared with some theoretical and experimental studies in Table 1.

The results of a Mulliken population analysis are shown in Table 2. The orbital populations for the C and O atoms for the free CO molecule and for the Pt atom in the free Pt atom and dimer are computed to C:2s^{1.80}2p^{1.86}, O:2s^{1.79}2p^{4.40}, Pt:6s^{1.00}5d^{8.99}6p^{0.00} and Pt:6s^{1.11}5d^{8.84}6p^{0.05}, respectively. By comparing the orbital populations before and after adsorption, one can obtain the nature of bonding between the CO molecule and the Pt atom and dimers.

Table 2 The results of Mulliken population analysis on the low-lying electronic states for the gas phase CO molecule and different configurations of the CO–Pt₂ (n = 1, 2) complexes.

| Molecule | 2S+1 | C | | | O | | | Pt ^a | | | Pt | | |
|----------------------------|------|----------|----------|----------|----------|----------|----------|-----------------|----------|----------|----------|----------|----------|
| | | <i>s</i> | <i>p</i> | <i>d</i> | <i>s</i> | <i>p</i> | <i>d</i> | <i>s</i> | <i>p</i> | <i>d</i> | <i>s</i> | <i>p</i> | <i>d</i> |
| CO | 1 | 1.799 | 1.862 | 0.078 | 1.792 | 4.395 | 0.060 | | | | | | |
| | 3 | 1.163 | 2.410 | 0.069 | 1.842 | 4.435 | 0.068 | | | | | | |
| CO-Pt | 1 | 1.308 | 2.243 | 0.118 | 1.827 | 4.462 | 0.064 | 1.033 | 0.014 | 8.876 | | | |
| | 3 | 1.461 | 2.209 | 0.106 | 1.823 | 4.425 | 0.063 | 0.907 | 0.244 | 8.725 | | | |
| CO-Pt ₂ Atop | 1 | 1.382 | 2.224 | 0.114 | 1.826 | 4.450 | 0.064 | 0.958 | 0.258 | 8.544 | 1.099 | 0.059 | 8.929 |
| | 3 | 1.409 | 2.203 | 0.111 | 1.825 | 4.439 | 0.064 | 0.964 | 0.268 | 8.503 | 1.334 | 0.060 | 8.710 |
| Bridge | 1 | 1.345 | 2.326 | 0.141 | 1.829 | 4.496 | 0.061 | 0.792 | 0.068 | 9.002 | 0.792 | 0.068 | 9.002 |
| | 3 | 1.342 | 2.333 | 0.136 | 1.830 | 4.469 | 0.062 | 1.105 | 0.113 | 8.660 | 1.105 | 0.118 | 8.659 |

^a Pt is connected to the CO molecule in the atop structures.

It is evident from Table 2 that after adsorption of the CO molecule on the Pt atom and dimer, the orbital population of C_{2s} is decreased, while the orbital population of C_{2p} is increased. Moreover, with respect to the oxygen population of the free CO molecule, the oxygen population in the *s* and *p* orbitals show a marginal increase, indicating a polarization of the C–O bond due to the interaction with the Pt atom and dimer.

In the CO–Pt complex, there is a transfer of 0.49*e* from 2*s* orbitals of the C atom to the 5*d* orbitals of the Pt atom, while the 5*d* orbitals of the Pt atom donate only 0.38*e* to the 2*π** orbitals of the C atom. In the case of CO–Pt₂ complex, the net transfer from the 2*s* orbitals of the C atom to the 5*d* orbitals of the Pt atoms is 0.42*e* (0.45*e*) for the atop (bridge) structure, while the back donation from the 5*d* orbitals of the Pt atoms to the anti-bonding 2*π** orbitals of the C atom is 0.36*e* (0.46*e*) for the atop (bridge) structure, respectively.

In the atop structure, the Pt atom participating in the bonding with the CO molecule loses more electronic density, while the other Pt atom slightly gains electronic density. However, in the bridge structure, the charge density is distributed equally on both the Pt atoms and they lose the same amount of charge density (see Table 2). For the bridge structure, the population of the Pt_{6s} orbital is considerably

decreased compared to the dissociated fragments, while the Pt_{5d} orbital population is increased which is consistent with the bonding picture between the Pt dimer and CO molecule.

As shown in Table 2, electron charge distribution on the CO molecule is not very sensitive to the spin state under consideration for both the CO–Pt and CO–Pt₂ complexes. However charge distribution on the Pt atoms and dimers vary with the spin state under consideration. The results of Mulliken population analysis are consistent with the results from vibrational frequency analysis. For example, the smallest *v*_{CO} is calculated for the bridge structure of the CO–Pt₂ complex, where the largest amount of back donation to the 2*π** orbitals of the CO molecule is calculated (Tables 1 and 2).

The electronic density of state (DOS) is also analyzed to further investigate the nature of interaction between the CO molecule and the Pt dimer. Figure 2b shows the total density of state (TDOS) of the Pt dimer and its individual contribution from the Pt_{6s} and the Pt_{5d} states. According to these DOS plots, the *s*–*d* hybridization does play an important role in maximizing the overlap between molecular orbitals in the Pt dimer. The asymmetric distribution of the majority (spin up) and minority (spin down) spins of the 5*d* states are mainly responsible for spin polarization and magnetic moment of 2*μ**B* for

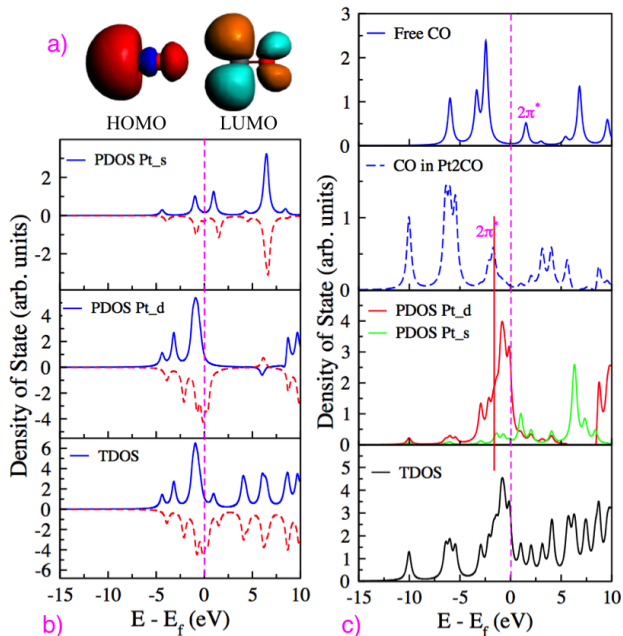


Figure 2 a) The HOMO and LUMO molecular orbitals of the CO molecule, b) Total density of states (TDOS) of the Pt dimer and partial density of states (PDOS) of the Pt_{6s} and Pt_{5d} states. The majority (blue line) and minority spins (red dash line) are also given. c) TDOS of the CO–Pt₂ complex and PDOS of the free and adsorbed CO molecule. PDOS of the Pt_{6s} and Pt_{5d} states are also given. The vertical pink dash line in each panel indicate the position of the Fermi level which is shifted to zero.

the Pt dimer.¹⁷ Moreover, when a CO molecule approaches the Pt dimer, the $6s$ occupation becomes less favorable, because of the Pauli repulsion between a diffuse $6s$ orbital of the Pt atom and the 5σ orbital of the CO molecule, and on the contrary the occupation of the inner shell $5d$ orbitals becomes more favorable due to the shielding of the Coulomb repulsion in these orbitals. Hence, the magnetic moment of the Pt dimer quenches to zero and the singlet state becomes the spin ground state of the CO–Pt₂ complex. The shift of the Pt_{6s} states toward higher energy in Figure 2c, which indicates less contribution to the occupied states, illustrates this phenomena. This also affects on the Pt–Pt bond distance, which increases from 2.36 Å (in the Pt dimer) to 2.55 Å (in the CO–Pt₂ complex), due

to loosing some contributions from the Pt_{6s} states. The hybridization between $5d$ states of the Pt dimer and $2\pi^*$ states of the CO molecule near the Fermi level are also illustrated in Figure 2c. The vertical red line is drawn as a guide to the eye to show the hybridization between $5d$ and $2\pi^*$ orbitals. The energy levels of the CO molecule are significantly shifted upward due to interaction with the Pt dimer. The Fermi level of the CO molecule is shifted from -9.02 eV (before adsorption) to -5.33 eV (after adsorption). It is noteworthy that the appearance of a new peak below the Fermi level is corresponding to relocation of electrons from the $5d$ orbital of the Pt atom to the $2\pi^*$ anti-bonding orbitals of the CO molecule.

CO adsorption on carbon-supported Pt atom and dimer

We recently studied the interaction of the Pt atom and dimer with a PAH surface on three highly symmetric adsorption sites of the PAH surface: the top site, above a carbon atom, the bridge site, between two neighboring carbon atoms, and the hollow site, surrounded by six carbon atoms, where it turns out that the bridge site is the most favorable adsorption site.¹⁷ Therefore, in the present work we investigate the adsorption of the CO molecule on the Pt atom and dimers located at the bridge adsorption sites of the PAH molecule.

To investigate the adsorption energy of the CO molecule on the supported Pt atom, the CO molecule is located on top of the Pt adatom (Figure 3a). After optimization, the CO molecule remains on top of the Pt adatom for the singlet state in a linear structure perpendicular to the PAH plane, whereas it is tilted out from the normal to the surface by 20° for the triplet state. The CO adsorption energy for the singlet state is -3.63 eV, which is more stable than for CO–Pt by only 0.03 eV. The triplet state is higher in energy at -1.96 eV. The C–O bond distance for the singlet state of the CO–Pt/PAH

complex is 1.162 Å which is longer than for the CO–Pt complex by 0.04 Å. The calculated ν_{CO} of 2023.8 cm^{-1} confirm the weakening of the C–O bond due to presence of the PAH substrate. The results are shown in Table 3.

For adsorption of the CO molecule on the Pt_2/PAH complex, we considered two different adsorption sites: linear (atop) and bridged structures. Considering two possible configurations for the Pt dimer on the PAH surface (parallel and perpendicular configurations), we have thus four configurations for adsorption of the CO molecule on the Pt_2/PAH complex (Figures 3b–e). The results are based on fixing the position of the Pt atoms along the x - and y -axes, i.e., in the surface plane, and relaxing the distance along the z -axis (perpendicular to the PAH surface), to study different possible configurations for interaction of the CO molecule with the adsorbed Pt dimer. However, after a complete relaxation of geometry, only the configurations in Figures 3b and 3d are stable. Moreover, no imaginary frequencies for these configurations are observed indicating they are stable minima on the potential energy surface.

The most stable configuration is found to be the configuration in Figure 3b, where the CO molecule is adsorbed on the bridge site of the parallel configuration of the Pt dimer. In this configuration, both the Pt atoms are in contact with the PAH surface and due to strong hybridization with the π orbitals of the PAH surface, they can both participate in charge transfer to the anti-bonding $2\pi^*$ orbital of the CO molecule. Generally, the PAH support has the capacity to accept electron density from Pt clusters,¹⁷ but it can also donate electrons when the CO molecule adsorbs to Pt atoms. In fact, the electron density surrounding metal particles has a major effect on their catalytic activity and the presence of the PAH substrate modulates the electron density. This particular feature of the PAH substrate is illustrated in the charge density difference plots, which will be discussed later.

The positive partial charge on the Pt atoms ($0.14e$)

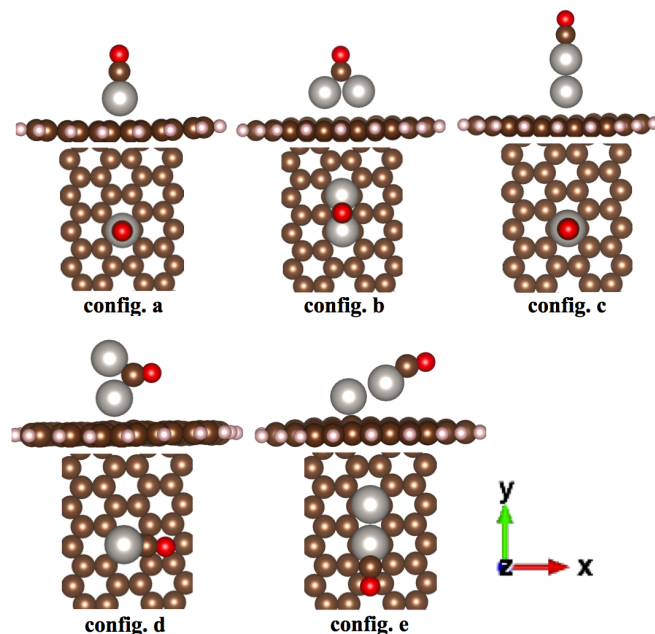


Figure 3 Top and side views of different configurations for adsorption of the CO molecule on the Pt_n/PAH ($n = 1, 2$) complex. b and d are the bridge configurations and the c and e are the atop configurations, respectively. Gray, brown, red and pink circles indicate Pt, C, O and H atoms, respectively.

bonded to the PAH surface results in receiving a large amount of electron density from the 5σ orbitals of the CO molecule by σ -donation, and the de-localized π electrons of the PAH support enhance the back donation to the anti-bonding $2\pi^*$ orbitals of the CO molecule. The weaker ν_{CO} of 1827.1 cm^{-1} reflects a stronger interaction between the CO molecule and the Pt dimer and consequently a stronger back donation. The Pt–C and C–O bond distances are calculated to 1.88 and 1.187 Å, respectively. The lower CO vibrational stretching frequency and the longer C–O bond length of this configuration (Figure 3b), in comparison to the CO binding to the substrate-free Pt dimer, also illustrates the impact of the PAH support in the adsorption of the CO molecule.

Despite the fact that the configuration in Figure 3c, was found to be the most stable configuration for adsorption of the Pt dimer on the PAH surface,¹⁷ it

is not the most favourable adsorption site for a CO molecule. The high electron density and negative partial charge on the upper Pt atom at the perpendicular Pt dimer, increase the repulsion between the 5σ orbital of the CO molecule and the $s-d$ orbitals of the Pt atom and consequently decrease the strength of the Pt–CO interaction. This repulsion is consistent with the direction of the dipole moment of the CO molecule with a small partial atomic charge on the C atom. Thus, CO adsorption becomes weaker for the atop site on the upper Pt adatom. In comparison with the other configurations (Table 3) and with the free Pt dimer (Tables 1), the relatively large value (2052.5 cm^{-1}) for ν_{CO} , reflects a weaker Pt–CO interaction. The C–O bond distance is calculated to 1.158 \AA for this configuration.

The second stable structure is the configuration in Figure 3d, where CO molecule is adsorbed on the bridge site of the perpendicular Pt dimer. The positive partial charge on the Pt atom bonded to the PAH surface, facilitates the electron transfer from the 5σ orbitals of the CO molecule to the $5d$ orbitals of the Pt adatom by σ -donation, and as seen from orbital population analyses (Table 4), some of the electron densities on the upper Pt atom is transferred to the anti-bonding $2\pi^*$ orbitals of the CO molecule by back donation. The C–O bond distance and the ν_{CO} for this structure are calculated to 1.185 \AA and 1843.4 cm^{-1} , respectively.

Another structure that we considered is the configuration in Figure 3e, where the CO molecule is adsorbed on the atop site of the parallel Pt dimer. Due to repulsion between the localized electron density on the O atom and the de-localized π electrons of the PAH surface, the CO molecule is tilted out from the surface and form a bent structure in relation to the Pt dimer. The Pt atom in contact with the CO molecule is slightly moved away from the surface due to interaction with the CO molecule. The Pt–PAH distance is calculated to 2.13 \AA for the Pt adatom bonded to the PAH surface. The ν_{CO} frequency is calculated to 2021.1 cm^{-1} , indicating a stronger interaction between Pt–CO as compared

to the atop structure in the substrate-free Pt dimer. The C–O bond distance is calculated to 1.162 \AA .

The results presented in Table 3 indicate that the CO adsorption for the bridge structures of the supported Pt dimer (Figures 3b and 3d) are stronger than for the atop structures (Figures 3c and 3e). This in agreement with the results from substrate free Pt dimer (Tables 1). The CO adsorption energy for the singlet state of the configurations in Figures 3b, 3c, 3d and 3e are calculated to -3.33 , -1.69 , -3.21 and -3.11 eV , respectively. Moreover, in comparison with the substrate-free Pt dimer (Tables 1), the adsorption energy for the CO binding to the Pt adatom far from the PAH surface (Figure 3c) is weaker and it is stronger when CO is adsorbed on Pt atoms connected to the PAH surface.

Therefore, it can be concluded that the PAH substrate significantly enhances the catalytic activity of the Pt adatoms for activating the CO molecule, where the reason is twofold: the positive partial charge on the Pt adatoms, due to interaction with the PAH surface, reduces the repulsion between the 5σ orbitals of the CO molecule and the $s-d$ orbitals of the Pt atom and facilitates the σ -donation from the 5σ orbitals of the CO molecule to the $5d$ orbitals of the Pt atoms. Secondly, the donation capability of electrons from the π orbitals of the PAH substrate enhances the back donation to the $2\pi^*$ orbitals of the CO molecule. This is also corroborated by the fact that the CO molecule is a strong π -acid. Cavallo *et al.* illuminated the key role of the π -acid CO ligand for promoting the reactivity of the Ru–olefin metathesis catalyst.⁸⁴

We also investigated the changes in the spin state and electronic structure of the PAH-supported Pt atom and dimer due to adsorption of the CO molecule. As shown in Figure 4, the spin ground state of the CO–Pt₂/PAH complex is the singlet state, and the triplet state is higher in energy for all configurations. The change from a triplet ground state to a singlet ground state due to interaction with the CO molecule was discussed above for the CO–Pt₂ complex. The spin multiplicity has a

Table 3 Results for the CO adsorption on the Pt_n/PAH ($n = 1, 2$) with configurations according to Figure 3. The CO adsorption energy, E_{ads} , the height of the Pt atom with respect to the averaged z coordinates of the C atoms in the PAH molecule, $d_{\text{Pt-PAH}}$, the distance between the Pt atom and the C_{CO} , $d_{\text{Pt-C}}$, the CO bond length, $d_{\text{C-O}}$, the vibrational stretching frequency of CO, ν_{CO} , the Hirshfeld atomic charge of Pt atoms, and the calculated $\langle S^2 \rangle$ values for different spin multiplicities ($2S + 1$) of the $\text{CO-Pt}_n/\text{PAH}$ ($n = 1, 2$) complexes are given. The values in parentheses for the configurations c, d, and e are the atomic charges related to the Pt atoms further from the PAH surface.

| config. | $2s+1$ | E_{ads} (eV) | $d_{\text{Pt-PAH}}$ (Å) | $d_{\text{Pt-C}}$ (Å) | $d_{\text{C-O}}$ (Å) | ν_{CO} (cm^{-1}) | Pt charge (e) | $\langle S^2 \rangle$ |
|---------|--------|----------------|-------------------------|-----------------------|----------------------|--|-------------------|-----------------------|
| a | 1 | -3.63 | 2.52 | 1.78 | 1.162 | 2023.8 | 0.11 | 0.00 |
| | 3 | -1.96 | 2.52 | 1.79 | 1.161 | 2019.6 | 0.12 | 2.00 |
| b | 1 | -3.33 | 2.78 | 1.88 | 1.187 | 1827.1 | 0.14(0.14) | 0.00 |
| | 3 | -2.51 | 2.82 | 1.92 | 1.181 | 1877.1 | 0.10(0.10) | 2.00 |
| c | 1 | -1.69 | 2.85 | 1.82 | 1.159 | 2052.5 | 0.11(-0.10) | 0.10 |
| | 3 | -1.49 | 2.53 | 1.84 | 1.158 | 2047.4 | 0.08(-0.06) | 2.00 |
| d | 1 | -3.21 | 2.18 | 1.88 | 1.185 | 1843.4 | 0.19(0.04) | 0.00 |
| | 3 | -1.98 | 2.20 | 1.91 | 1.184 | 1851.1 | 0.18(-0.04) | 2.00 |
| e | 1 | -3.11 | 2.13 | 1.78 | 1.162 | 2021.1 | 0.14(0.02) | 0.00 |
| | 3 | -2.30 | 2.29 | 1.80 | 1.160 | 2005.8 | 0.11(-0.02) | 2.00 |

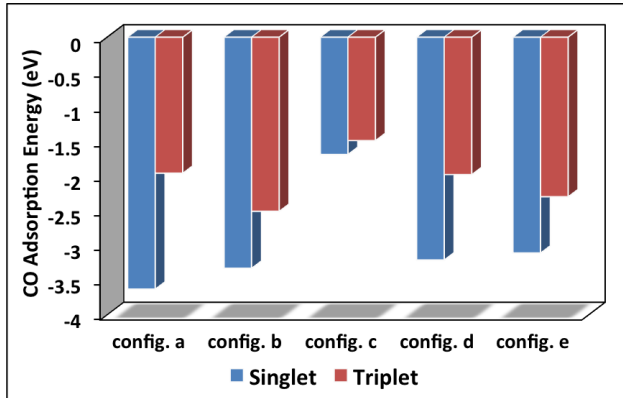


Figure 4 Singlet-triplet excitation energy for the CO adsorption on the PAH-supported Pt atom and Pt dimer.

large effect on structural, electronic and vibrational properties of the $\text{CO-Pt}_2/\text{PAH}$ complex. At all adsorption configurations, changing the spin state from the singlet state to the triplet state, accompanied with changing the orbital population in the Pt adatoms, in which the population of outer shells ($6s$ and $6p$) is increased (Table 4). The Pt-CO interaction is, therefore, quenched due to increasing the

Pauli repulsion between the $6s - p$ states of the Pt adatom and the lone-pair 5σ orbitals of the CO molecule, and consequently the adsorption energies become weaker for the triplet state. The C-O bond distances are also shorter for the triplet state as compared to the singlet state.

The degree of spin contamination is checked by comparing the expectation value, $\langle S^2 \rangle$, with the ideal value, $S(S+1)$, as seen in Tables 1 and 3. A small deviation of $\langle S^2 \rangle$ from the ideal value confirms the good performance of the S12g functional for studying spin states of transition metal complexes.^{32,38}

The results of the Mulliken population analysis for various atoms at the $\text{CO-Pt}_n/\text{PAH}$ complexes are shown in Table 4. Comparing the orbital populations of the supported Pt atom and dimer and the CO molecule before and after adsorption, gives us the characteristic features of bonding between the CO molecule and the supported Pt atom and dimers. For all configurations, as for the substrate-free Pt atom and dimer, the population of the $2s$ orbital of

Table 4 The results of Mulliken population analysis on the low-lying electronic states for different configurations of the CO–Pt_n/PAH (n=1, 2) complex, according to Figure 3.

| config. | 2S+1 | C | | | O | | | Pt ^a | | | Pt ^b | | |
|---------|------|----------|----------|----------|----------|----------|----------|-----------------|----------|----------|-----------------|----------|----------|
| | | <i>s</i> | <i>p</i> | <i>d</i> | <i>s</i> | <i>p</i> | <i>d</i> | <i>s</i> | <i>p</i> | <i>d</i> | <i>s</i> | <i>p</i> | <i>d</i> |
| a | 1 | 1.385 | 2.279 | 0.078 | 1.819 | 4.496 | 0.060 | 0.793 | 0.250 | 8.707 | | | |
| | 3 | 1.393 | 2.272 | 0.119 | 1.820 | 4.485 | 0.061 | 0.767 | 0.260 | 8.698 | | | |
| b | 1 | 1.368 | 2.452 | 0.140 | 1.835 | 4.492 | 0.060 | 0.734 | 0.140 | 9.000 | 0.741 | 0.134 | 9.000 |
| | 3 | 1.391 | 2.505 | 0.138 | 1.837 | 4.487 | 0.062 | 1.135 | 0.176 | 8.674 | 1.143 | 0.172 | 8.671 |
| c | 1 | 1.534 | 2.227 | 0.114 | 1.822 | 4.472 | 0.064 | 0.640 | 0.383 | 8.455 | 1.241 | 0.200 | 8.962 |
| | 3 | 1.527 | 2.199 | 0.110 | 1.821 | 4.467 | 0.062 | 1.041 | 0.257 | 8.526 | 1.382 | 0.134 | 8.757 |
| d | 1 | 1.492 | 2.381 | 0.114 | 1.836 | 4.489 | 0.064 | 0.741 | 0.180 | 8.799 | 0.959 | 0.099 | 8.873 |
| | 3 | 1.487 | 2.386 | 0.096 | 1.815 | 4.476 | 0.033 | 0.876 | 0.212 | 8.463 | 1.177 | 0.169 | 8.575 |
| e | 1 | 1.470 | 2.290 | 0.114 | 1.844 | 4.471 | 0.064 | 0.890 | 0.080 | 8.948 | 0.931 | 0.239 | 8.585 |
| | 3 | 1.476 | 2.294 | 0.107 | 1.838 | 4.464 | 0.062 | 0.985 | 0.183 | 8.731 | 1.108 | 0.265 | 8.461 |

^a Pt adatom is connected to the PAH surface.

^b Pt adatom is far from the PAH surface for the c, d and e configurations.

the carbon atom is decreased due to donation of electrons to the 5*d* orbitals of the Pt atom, while the orbital population of the 2*p* orbitals of the carbon atom is increased because of back donation from 5*d* orbitals of the Pt adatoms to the 2*π** orbitals of the CO molecule. Moreover, increasing the population of the *s* and *p* orbitals of the oxygen atom as compared to the free CO molecule indicates a polarization of the C–O bond after adsorption on the supported Pt atom and dimer.

To highlight the impact of the PAH support on adsorption of the CO molecule, it is worth comparing the orbital populations and the amount of electron transfer to/from the CO molecule on the substrate-free and carbon-supported Pt dimer. For example, in the most stable configuration of the CO–Pt₂/PAH (Figure 3b), the net amount of electron transferred from the 2*s* orbitals of the C atom to the 5*d* orbitals of the Pt atoms is 0.43*e*, and the back donation from the 5*d* orbitals of the Pt atoms to the anti-bonding 2*π** orbitals of the C atom is 0.54*e*, while for the most stable structure of the CO–Pt₂ complex (bridge structure), the corresponding values are 0.45*e* and 0.46*e*, respectively. Hence the net amount of electron transfer to the

anti-bonding 2*π** orbitals of the CO molecule is higher in the carbon-supported Pt dimer than for the substrate-free Pt dimer which is also reflected in a lower vibrational frequency and a larger C–O bond distance for the CO–Pt₂/PAH complex. This is showing the significant contribution from the PAH support on the adsorption of the CO molecule by enhancing the back donation of electrons to the 2*π** orbitals of the CO molecule.

Moreover, comparing the partial Hirshfeld charges on the carbon atoms in the PAH connected to the Pt adatoms, before and after adsorption of the CO molecule, results in a small transfer of electrons from the carbon support to the Pt adatoms. For example, for the configuration in Figure 3b, the partial charges for the carbon atoms connected to the Pt adatoms were –0.024*e*, while this value changed to –0.011*e*, after adsorption of the CO molecule.

Generally, the additional bonds from the Pt atoms to the PAH support may reduce the under-coordination, which is responsible for the surprisingly high reactivity of the atom-type Pt catalysts.^{4,85} However, donation capability of electrons from the *π* orbitals of the PAH substrate, enhances the back donation of electrons to the 2*π** orbitals of the CO molecule

and strengthens the Pt–CO interaction. Sun *et al.* reported that the atom-type Pt catalyst on graphene surface exhibit higher activity (up to 10 times) for methanol oxidation and superior CO tolerance than the conventional Pt/C catalyst.⁴ Using X-ray absorption fine structure analyses, they showed that the low-coordination and partially unoccupied densities of states of the Pt $5d$ orbitals are responsible for the excellent performance. Therefore, CO adsorption energy on atom-type Pt catalysts is generally greater than that on Pt particles and their corresponding extended surfaces.^{86,87}

We also investigated the CDD for all configura-

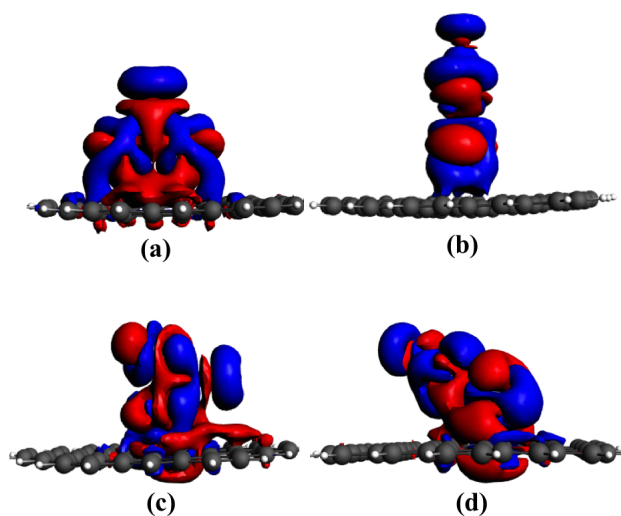


Figure 5 The calculated charge density differences for adsorption of the CO molecule on the PAH-supported Pt dimer. The a, b, c, and d plots are correspond to the configurations b, c, d and e in Figure 3, respectively. The blue and red contours indicate the areas of the charge accumulation and depletion, respectively. The same iso-value of 0.0003 a.u. was employed for all contours.

tions of the CO–Pt₂/PAH complex (Figure 5). The strong variation in the charge density at the interface is due to the interaction with the PAH surface. The iso-surfaces show enhancement of charge density (blue map) around the Pt–PAH and the Pt–C bonds. There is also an accumulation of charge density on the oxygen atom and a depletion of charge density (red map) on the C atom of the CO

molecule. A red iso-surface surrounding the PAH substrate indicates a depletion of the charge density on the π orbitals of the PAH surface when the CO molecule adsorbes. This observation is corroborated by the Mulliken population analysis (Table 4).

Figure 6 shows the DOS plots from different configurations of the CO–Pt₂/PAH complex. For all configurations, the energy levels of the CO molecule are significantly shifted due to adsorption to the Pt₂/PAH, and the new states appearing below the Fermi level correspond to relocation of electrons to the $2\pi^*$ anti-bonding orbitals of the CO molecule. These states were also present in the DOS plots of the CO molecule interacting with the substrate-free Pt dimer, but here the states are shifted slightly upward due to interaction with the PAH orbitals, and the peaks are larger indicating that more electrons are relocated to the $2\pi^*$ orbitals of CO molecule. This clearly illustrates the influence of the PAH support on the CO activation and it is consistent with the results from the Mulliken population (Table 4) and the vibrational stretching frequencies (Table 3). The DOS spectrums show that the $5d$ orbital of the Pt adatom and the $2\pi^*$ orbital of the CO molecule, which are mainly responsible for the Pt–CO interaction, are in the same energy scale below the Fermi level and the strength of the Pt–CO interaction depends on the strength of the overlap between these states. The vertical red line in each panel is drawn as a guide to the eye to show the hybridization between $5d$ and $2\pi^*$ orbitals. For example, the DOS plots in Figures 6a and 6b correspond to the most and the least stable configurations (Figures 3b and 3c, respectively) for the CO–Pt₂/PAH complexes, where the amount of overlap between the $5d$ and $2\pi^*$ orbitals are the largest and the smallest, respectively. Moreover, the amount of contribution from the Pt_{6s}, which is a source of the repulsion with the 5σ orbitals of the CO molecule, in the hybridization below the Fermi level, are again the smallest and the largest for explained configurations, respectively. Therefore, changing the chemical surrounding of the $5d$ states by the PAH support leads

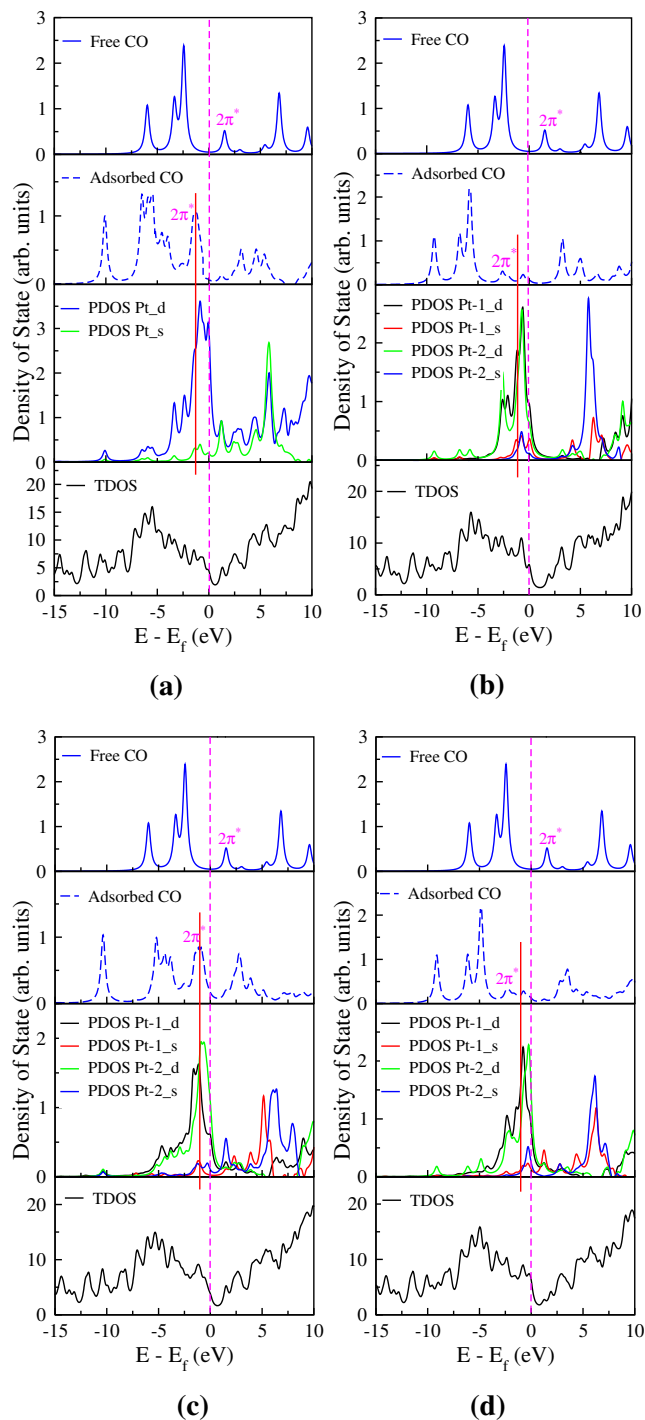


Figure 6 Total density of states (TDOS) and partial density of states (PDOS) of the CO molecule before and after adsorption on different configurations of the CO–Pt₂/PAH complex. TDOS of the CO–Pt₂/PAH for all configurations and PDOS from the *s* and *d* orbitals are also given. The a, b, c, and d plots correspond to the configurations b, c, d and e in Figure 3, respectively. The vertical pink dash line in each panel indicate the position of the Fermi level which is shifted to zero.

to significantly change in the hybridization features between *5d* and $2\pi^*$ orbitals and consequently in the adsorption characteristics of the CO molecule.

Conclusions

Density functional theory calculations were used to characterize the influence of carbon support on adsorption of the CO molecule on the Pt atom and dimer. CO adsorption energies have been calculated for different configurations on the PAH-supported and substrate-free Pt atom and dimer. The results have been discussed based on the adsorption sites, molecular orbital populations, vibrational frequencies, charge transfer in terms of partial atomic charges, charge density differences and the projected density of states. Our results show that the presence of the PAH surface changes the electron density distribution around the Pt adatoms since the carbon support enhances the back donation of electrons to the $2\pi^*$ orbitals of the CO molecule and consequently enhances the catalytic activity of the Pt adatoms in contact with the PAH surface as compared to the substrate-free Pt atoms. Hybridization between the π orbitals of the PAH surface and the *d* orbitals of the Pt adatoms is responsible for this effect which results in a larger peak below the Fermi level for the $2\pi^*$ states of the CO molecule in the corresponding DOS plots. While the high electron density and the partial negative charge on the Pt atoms not directly bonded to the PAH surface, increase the repulsion between the 5σ orbital of the CO molecule and the *s-d* orbitals of the Pt adatom and consequently reduces the Pt–CO interaction. This results in a higher vibrational stretching frequency for the CO molecule, compared to the substrate-free Pt atoms, and a smaller peak below the Fermi level for the $2\pi^*$ states of the CO molecule in the corresponding DOS plots.

Therefore, changing the chemical surrounding of the

$5d$ states of the Pt atoms by the PAH support leads to significantly change in the hybridization features between $5d$ and $2\pi^*$ orbitals and consequently in the adsorption characteristics of the CO molecule. By further modulating the electron density of the carbon support (by adding defects, dopants, edge functional groups, etc.), one may design the catalytic activity of the atom-type Pt catalysts.

Acknowledgment

This work is a part of the ISP project (209337) with financial support from the Norwegian Research Council. Computational time provided by the Notur project (account 2920k) is acknowledged.

References

- (1) Bell, A. The Impact of Nanoscience on Heterogeneous Catalysis. *Science* **2003**, *299*, 1688–1691.
- (2) Basri, S.; Kamarudin, S.; Daud, W.; Yaakub, Z. Nanocatalyst for Direct Methanol Fuel Cell (DMFC). *Int. J. Hydrogen Energy* **2010**, *35*, 7957–7970.
- (3) Wang, X.; Wang, S. In *Materials for Low-Temperature Fuel Cells*, 1st ed.; Ladewig, B., Jiang, S. P., Yan, Y., Eds.; Wiley: Germany, 2015; Chapter 3.
- (4) Sun, S.; Zhang, G.; Gauquelin, N.; Chen, N.; Zhou, J.; Yang, S.; Chen, W.; Meng, X.; Geng, D.; Bannis, M. N. et al. Single-Atom Catalysis Using Pt/Graphene Achieved Through Atomic Layer Deposition. *Sci. Rep.* **2013**, *3*.
- (5) Liang, S.; Hao, C.; Shi, Y. The Power of Single-Atom Catalysis. *ChemCatChem* **2015**, *7*, 2559–2567.
- (6) Yang, X.-F.; Wang, A.; Qiao, B.; Li, J.; Liu, J.; Zhang, T. Single-Atom Catalysts: A New Frontier in Heterogeneous Catalysis. *Acc. Chem. Res.* **2013**, *46*, 1740–1748.
- (7) Scheuermann, G. M.; Rumi, L.; Steurer, P.; Bannwarth, W.; Mühlaupt, R. Palladium Nanoparticles on Graphite Oxide and Its Functionalized Graphene Derivatives as Highly Active Catalysts for the Suzuki-Miyaura Coupling Reaction. *J. Am. Chem. Soc.* **2009**, *131*, 8262–8270.
- (8) Tang, L.; Wang, Y.; Li, Y.; Feng, H.; Lu, J.; Li, J. Preparation, Structure, and Electrochemical Properties of Reduced Graphene Sheet Films. *Adv. Funct. Mater.* **2009**, *19*, 2782–2789.
- (9) Yoo, E.; Okata, T.; Akita, T.; Kohyama, M.; Nakamura, J.; Honma, I. Enhanced Electrocatalytic Activity of Pt Subnanoclusters on Graphene Nanosheet Surface. *Nano Lett.* **2009**, *9*, 2255–2259.
- (10) Gan, Y.; Sun, L.; Banhart, F. One- and Two-Dimensional Diffusion of Metal Atoms in Graphene. *Small* **2008**, *4*, 587–591.
- (11) Xu, C.; Wang, X.; Zhu, J. Graphene-Metal Particle Nanocomposites. *J. Phys. Chem. C* **2008**, *112*, 19841–19845.
- (12) Muszynski, R.; Seger, B.; Kamat, P. V. Decorating Graphene Sheets with Gold Nanoparticles. *J. Phys. Chem. C* **2008**, *112*, 5263–5266.
- (13) Schanke, D.; Vada, S.; Blekkan, E. A.; Hilmen, A. M.; Hoff, A.; Holmen, A. Study of Pt-Promoted Cobalt CO Hydrogenation Catalysts. *J. Catal.* **1995**, *156*, 85–95.
- (14) Vada, S.; Hoff, A.; Ådnanes, E.; Schanke, D.; Holmen, A. Fischer-Tropsch Synthesis on Supported Cobalt Catalysts Promoted by Platinum and Rhenium. *Top. Catal.* **1995**, *2*, 155–162.
- (15) Dees, M. J.; Ponec, V. The Influence of Sulfur and Carbonaceous Deposits on the Selectivity and Activity of Pt/Co Catalysts in Hydrocarbon Reactions. *J. Catal.* **1989**, *119*, 376–387.
- (16) Cheng, H.-Y.; Åstrand, P.-O.; Chen, D.; Zhu, Y.-A.; Zhou, X.-G.; Li, P. Adsorption of a Single Pt Atom on Polyaromatic Hydrocarbons from First-Principle Calculations. *Chem. Phys. Lett.* **2013**, *575*, 76–80.
- (17) Mahmoodinia, M.; Ebadi, M.; Åstrand, P.-O.; Chen, D.; Cheng, H.-Y.; Zhu, Y.-A. Structural and Electronic Properties of the Pt_n-PAH Complex (*n* = 1, 2) from Density Functional Calculations. *Phys. Chem. Chem. Phys.* **2014**, *16*, 18586–18595.
- (18) Mahmoodinia, M.; Åstrand, P.-O.; Chen, D. Chemical Bonding and Electronic Properties of the Co Adatom and Dimer Interacting with Polyaromatic Hydrocarbons. *J. Phys. Chem. C* **2015**, *119*, 24425–24438.
- (19) Fampiou, I.; Ramasubramanian, A. Binding of Pt Nanostructures to Point Defects in Graphene: Adsorption, Morphology, and Electronic Structure. *J. Phys. Chem. C* **2012**, *116*, 6543–6555.
- (20) Sanz-Navarro, C. F.; Åstrand, P.-O.; Chen, D.; Rønning, M.; van Duin, A. C. T.; Jacob, T.; Goddard, W. A. Molecular Dynamics Simulations of the Interactions between Platinum Clusters and Carbon Platelets. *J. Phys. Chem. A* **2008**, *112*, 1392–1402.
- (21) Müller, U.; Sattler, K.; Xhie, J.; Venkateswaran, N.; Raina, G. Scanning Tunneling Microscopy of Single Platinum Atoms and Small Platinum Clusters on Highly Oriented Pyrolytic Graphite. *J. Vac. Sci. Technol. B* **1991**, *9*, 829–832.
- (22) Wang, Q. J.; Che, J. G. Origins of Distinctly Different Behaviors of Pd and Pt Contacts on Graphene. *Phys. Rev. Lett.* **2009**, *103*.
- (23) Chan, K. T.; Neaton, J. B.; Cohen, M. L. First Principles Study of Metal Adatom Adsorption on Graphene. *Phys. Rev. B: Condens. Matter Mater. Phys.* **2008**, *77*.
- (24) Ogletree, D. F.; van Hove, M. A.; Somorjai, G. A. LEED Intensity Analysis of the Structures of Clean Pt(111) and of CO Adsorbed on Pt(111) in the C(4×2) Arrangement. *Surf. Sci.* **1986**, *173*, 351–365.
- (25) Blackman, G.; Xu, M.-L.; Ogletree, D. F.; Hove, M. A. V.; Somorjai, G. A. Mix of Molecular Adsorption Sites Detected for Disordered CO on Pt(111) by Diffuse Low-Energy Electron Diffraction. *Phys. Rev. Lett.* **1988**, *61*, 2352–2355.
- (26) Hopster, H.; Ibach, H. Adsorption of CO on Pt(111) and Pt 6(111) × (111) Studied by High Resolution Electron Energy Loss Spectroscopy and Thermal Desorption Spectroscopy. *Surf. Sci.* **1978**, *77*, 109–117.
- (27) Bocquet, M.-L.; Sautet, P. STM and Chemistry: A Qualitative Molecular Orbital Understanding of the Image of CO on a Pt Surface. *Surf. Sci.* **1996**, *360*, 128–136.

- (28) Kim, Y. D.; Boo, J.-H.; Lee, S.-B. Adsorption Behaviors of CO on W(110) and Mo(110) Surfaces in the β -state Are Still Not Clear. *Surf. Sci.* **2009**, *603*, 1434–1438.
- (29) Cao, Z.; Wang, Y.; Zhu, J.; Wu, W.; Zhang, Q. Static Polarizabilities of Copper Cluster Monocarbonyls Cu_nCO ($n = 2-13$) and Selectivity of CO Adsorption on Copper Clusters. *J. Phys. Chem. B* **2002**, *106*, 9649–9654.
- (30) Poater, A.; Duran, M.; Jaque, P.; Toro-Labbé, A.; Solà, M. Molecular Structure and Bonding of Copper Cluster Monocarbonyls Cu_nCO ($n = 1-9$). *J. Phys. Chem. B* **2006**, *110*, 6526–6536.
- (31) Grushow, A.; Ervina, K. M. Ligand and Metal Binding Energies in Platinum Carbonyl Cluster Anions: Collision-Induced Dissociation of Pt_m^- and $\text{Pt}_m(\text{CO})_n^-$. *J. Chem. Phys.* **1997**, *106*, 9580–9593.
- (32) Swart, M. A New Family of Hybrid Density Functionals. *Chem. Phys. Lett.* **2013**, *580*, 166–171.
- (33) Velde, G. T.; Bickelhaupt, F. M.; Baerends, E. J.; Guerra, C. F.; van Gisbergen, S. J. A.; Snijders, J. G.; Ziegler, T. Chemistry with ADF. *J. Comput. Chem.* **2001**, *22*, 931–967.
- (34) Guerra, C. F.; Snijders, J. G.; Velde, G. T.; Baerends, E. J. Towards an Order-N DFT Method. *Theor. Chem. Acc.* **1998**, *99*, 391–403.
- (35) Swart, M.; Solà, M.; Bickelhaupt, F. M. Switching Between OPTX and PBE Exchange Functionals. *J. Comput. Meth. Sci. Engin.* **2009**, *9*, 69–77.
- (36) Swart, M.; Solà, M.; Bickelhaupt, F. M. A New All-Round Density Functional Based on Spin States and SN_2 Barriers. *J. Chem. Phys.* **2009**, *131*.
- (37) Grimme, S. Density Functional Theory with London Dispersion Corrections. *WIREs Comput. Mol. Sci.* **2011**, *1*, 211–228.
- (38) Gruden-Pavlović, M.; Stepanović, S.; Perić, M.; Güell, M.; Swart, M. A Density Functional Study of the Spin State Energetics of Polypyrazolylborato Complexes of First-Row Transition Metals. *Phys. Chem. Chem. Phys.* **2014**, *16*, 14514–14522.
- (39) Heully, J. L.; Lindgren, I.; Lindroth, E.; Lundqvist, S.; Martensson-Pendrill, A. M. Diagonalisation of the Dirac Hamiltonian as a Basis for a Relativistic Many-Body Procedure. *J. Phys. B: At. Mol. Phys.* **1986**, *19*, 2799–2815.
- (40) van Lenthe, E.; Baerends, E. J.; Snijders, J. G. Relativistic Regular Two-Component Hamiltonians. *J. Chem. Phys.* **1993**, *99*, 4597–4610.
- (41) van Lenthe, E.; Baerends, E. J.; Snijders, J. G. Relativistic Total Energy Using Regular Approximations. *J. Chem. Phys.* **1994**, *101*, 9783–9792.
- (42) van Lenthe, E.; Snijders, J.; Baerends, E. The Zero-Order Regular Approximation for Relativistic Effects: The Effect of Spin-Orbit Coupling in Closed Shell Molecules. *J. Chem. Phys.* **1996**, *105*, 6505–6516.
- (43) van Lenthe, E.; van Leeuwen, R.; Baerends, E. J.; Snijders, J. G. Relativistic Regular Two-Component Hamiltonians. *Int. J. Quantum Chem.* **1996**, *57*, 281–293.
- (44) van Lenthe, E.; Ehlers, A.; Baerends, E. Geometry Optimization in the Zero Order Regular Approximation for Relativistic Effects. *J. Chem. Phys.* **1999**, *110*, 8943–8953.
- (45) Schlegel, H. B. *Ab-Initio Methods in Quantum Chemistry*; Wiley: New York, 1987; Vol. I.
- (46) Boys, S. F.; Bernardi, F. The Calculation of Small Molecular Interactions by the Differences of Separate Total Energies. Some Procedures with Reduced Errors. *Mol. Phys.* **1970**, *19*, 553–566.
- (47) Mulliken, R. S. Electronic Population Analysis on LCAO-MO Molecular Wave Functions. I. *J. Chem. Phys.* **1955**, *23*, 1833–1840.
- (48) Mulliken, R. S. Electronic Population Analysis on LCAO-MO Molecular Wave Functions. IV. Bonding and Antibonding in LCAO and Valence-Bond Theories. *J. Chem. Phys.* **1955**, *23*, 2343–2346.
- (49) Kittel, C.; McFadden, P. *Introduction to Solid State Physics*, 8th ed.; Wiley: New York, 1976.
- (50) Hirshfeld, F. L. Bonded-Atom Fragments for Describing Molecular Charge Densities. *Theor. Chim. Acta* **1977**, *44*, 129–138.
- (51) Wiberg, K. B.; Rablen, P. R. Comparison of Atomic Charges Derived via Different Procedures. *J. Comput. Chem.* **1993**, *14*, 1504–1518.
- (52) Sheng, L.; Ono, Y.; Taketsugu, T. Ab Initio Study of Xe Adsorption on Graphene. *J. Phys. Chem. C* **2010**, *114*, 3544–3548.
- (53) Kim, C. K.; Park, B. H.; Park, S. J.; Kim, C. K. Modeling Studies on the Uptake of Hydrogen Molecules by Graphene. *J. Mol. Model.* **2015**, *21*.
- (54) Fowler, P. W.; Gibson, C. M.; Bean, D. E. Writing with Ring Currents: Selectively Hydrogenated Polycyclic Aromatics as Finite Models of Graphene and Graphane. *Proc. R. Soc. A* **2014**, *470*.
- (55) van Lenthe, E.; Baerends, E. J. Optimized Slater-Type Basis Sets for the Elements 1-118. *J. Comput. Chem.* **2003**, *24*, 1142–1156.
- (56) Schimka, L.; Harl, J.; Stroppa, A.; Grüneis, A.; Marsman, M.; Mittendorfer, F.; Kresse, G. Accurate Surface and Adsorption Energies From Many-Body Perturbation Theory. *Nature Mater.* **2010**, *9*, 741–744.
- (57) Zeinalipour-Yazdi, C. D.; Cooksy, A. L.; Efstathiou, A. M. CO Adsorption on Transition Metal Clusters: Trends from Density Functional Theory. *Surf. Sci.* **2008**, *602*, 1858–1862.

- (58) Gil, A.; Clotet, A.; Ricart, J. M.; Kresse, G.; García-Hernández, M.; Rösch, N.; Sautet, P. Site Preference of CO Chemisorbed on Pt(111) From Density Functional Calculations. *Surf. Sci.* **2003**, *530*, 71–76.
- (59) Geschke, D.; Baştuğ, T.; Jacob, T.; Fritzsche, S.; Sepp, W.-D.; Fricke, B.; Varga, S.; Anton, J. Adsorption of CO on Cluster Models of Platinum (111): A Four-Component Relativistic Density-Functional Approach. *Phys. Rev. B: Condens. Matter Mater. Phys.* **2001**, *64*.
- (60) Orita, H.; Itoh, N.; Inada, Y. All Electron Scalar Relativistic Calculations on Adsorption of CO on Pt(111) with Full-Geometry Optimization: A Correct Estimation for CO Site-Preference. *Chem. Phys. Lett.* **2004**, *384*, 271–276.
- (61) Dewar, M. J. S. A Review of π Complex Theory. *Bull. Soc. Chim. Fr.* **1951**, *18*, C79.
- (62) Chatt, J.; Duncanson, L. A. Olefin Co-ordination Compounds. Part III. Infra-Red Spectra and Structure: Attempted Preparation of Acetylene Complexes. *J. Chem. Soc.* **1953**, 2939–2947.
- (63) Chatt, J.; Duncanson, L. A.; Venanzi, L. M. Directing Effects in Inorganic Substitution Reactions. Part I. A Hypothesis to Explain the Trans-Effect. *J. Chem. Soc.* **1955**, 4456–4460.
- (64) Mingos, D. M. P. A Historical Perspective on Dewar's Landmark Contribution to Organometallic Chemistry. *J. Organomet. Chem.* **2001**, *635*, 1–8.
- (65) Blyholder, G. Molecular Orbital View of Chemisorbed Carbon Monoxide. *J. Phys. Chem.* **1964**, *68*, 2772–2777.
- (66) Apai, G.; Wehner, P. S.; Williams, R. S.; Stöhr, J.; Shirley, D. A. Orientation of CO on Pt(111) and Ni(111) Surfaces from Angle-Resolved Photoemission. *Phys. Rev. Lett.* **1976**, *37*, 1497–1500.
- (67) Goldman, A. S.; Krogh-Jespersen, K. Why Do Cationic Carbon Monoxide Complexes Have High C–O Stretching Force Constants and Short C–O Bonds? Electrostatic Effects, Not σ -Bonding. *J. Am. Chem. Soc.* **1996**, *118*, 12159–12166.
- (68) Frenking, G.; Fröhlich, N. The Nature of the Bonding in Transition-Metal Compounds. *Chem. Rev.* **2000**, *100*, 717–774.
- (69) Zhou, M.; Andrews, L.; Bauschlicher Jr., C. W. Spectroscopic and Theoretical Investigations of Vibrational Frequencies in Binary Unsaturated Transition-Metal Carbonyl Cations, Neutrals, and Anions. *Chem. Rev.* **2001**, *101*, 1931–1961.
- (70) Lupinetti, A. J.; Fau, S.; Frenking, G.; Strauss, S. H. Theoretical Analysis of the Bonding between CO and Positively Charged Atoms. *J. Phys. Chem. A* **1997**, *101*, 9551–9559.
- (71) Lupinetti, A. J.; Frenking, G.; Strauss, S. H. Nonclassical Metal Carbonyls: Appropriate Definitions with a Theoretical Justification. *Angew. Chem., Int. Ed.* **1998**, *37*, 2113–2116.
- (72) Huber, K. P.; Herzberg, G. *Molecular Spectra and Molecular Structure IV: Constants of Diatomic Molecules*; Van Nostrand Reinhold Co: New York, 1979.
- (73) Nordling, C.; Österman, J. *Physics Handbook for Science and Engineering*; Studentlitteratur AB: Lund, 1980.
- (74) Yeo, Y. Y.; Vattuone, L.; King, D. A. Calorimetric Heats for CO and Oxygen Adsorption and for the Catalytic CO Oxidation Reaction on Pt(111). *J. Chem. Phys.* **1997**, *106*, 392–401.
- (75) Heyden, B. E.; Bradshaw, A. M. The Adsorption of CO on Pt(111) Studied by Infrared Reflection-Absorption Spectroscopy. *Surf. Sci.* **1983**, *125*, 787–802.
- (76) Roszak, S.; Balasubramanian, K. A Theoretical Study of Bridged vs Atop Interactions of Pt₂ with CO. *J. Chem. Phys.* **1995**, *103*, 1043–1049.
- (77) Muentzer, J. S. Electric Dipole Moment of Carbon Monoxide. *J. Mol. Spectrosc.* **1975**, *55*, 490–491.
- (78) Sadek, M. M.; Wang, L. Effect of Adsorption Site, Size, and Composition of Pt/Au Bimetallic Clusters on the CO Frequency: A Density Functional Theory Study. *J. Phys. Chem. A* **2006**, *110*, 14036–14042.
- (79) Sebetci, A. Interaction of Carbon Monoxide with Bimetallic Co-Pt Clusters: A Density Functional Theory Study. *Comput. Mater. Sci.* **2012**, *58*, 77–86.
- (80) Lazić, P.; Alaei, M.; Atodiresei, N.; Caciuc, V.; Brako, R.; Blügel, S. Density Functional Theory with Nonlocal Correlation: A Key to the Solution of the CO Adsorption Puzzle. *Phys. Rev. B: Condens. Matter Mater. Phys.* **2010**, *81*.
- (81) Norton, P. R.; Davies, J. A.; Jackman, T. E. Absolute Coverage and Isosteric Heat of Adsorption of Deuterium on Pt(111) Studied by Nuclear Microanalysis. *Surf. Sci.* **1982**, *121*, 103–110.
- (82) Baró, A. M.; Ibach, H. New Study of CO Adsorption at Low Temperature (90 K) on Pt(111) by EELS. *J. Chem. Phys.* **1979**, *71*, 4812–4816.
- (83) Crossley, A.; King, D. A. Adsorbate Island Dimensions and Interaction Energies From Vibrational Spectra: CO on Pt (001) and Pt (111). *Surf. Sci.* **1980**, *95*, 131–155.
- (84) Poater, A.; Ragone, F.; Correa, A.; Cavallo, L. Exploring the Reactivity of Ru-Based Metathesis Catalysts with a π -Acid Ligand Trans to the Ru-Ylidene Bond. *J. Am. Chem. Soc.* **2009**, *131*, 9000–9006.
- (85) Russell, J.; Zapol, P.; Král, P.; Curtiss, L. A. Methane Bond Activation by Pt and Pd Subnanometer Clusters Supported on Graphene and Carbon Nanotubes. *Chem. Phys. Lett.* **2012**, *536*, 9–13.

-
- (86) Xu, Y.; Getman, R. B.; Shelton, W. A.; Schneider, W. F. A First-Principles Investigation of the Effect of Pt Cluster Size on CO and NO Oxidation Intermediates and Energetics. *Phys. Chem. Chem. Phys.* **2008**, *10*, 6009–6018.
- (87) Bourane, A.; Dulaurent, O.; Bianchi, D. Heats of Adsorption of Linear and Multibound Adsorbed CO Species on a Pt/Al₂O₃ Catalyst Using in Situ Infrared Spectroscopy Under Adsorption Equilibrium. *J. Catal.* **2000**, *196*, 115–125.

Graphical TOC Entry

